Design, Modeling and Control of a Spherical Autonomous Underwater Vehicle for Mine Exploration*

Ramon A. Suarez Fernandez[1], E. Andres Parra R.[1], Sergio Dominguez[1] and Claudio Rossi[1]

***Abstract*— This paper presents the design, implementation and validation of a novel spherical Autonomous Underwater Vehicle (AUV) prototype, developed for inspection and exploration of flooded mine tunnel networks. The unique mechanical, electrical and hardware design is presented, as well as the development of a theoretical 6 degree-of-freedom (DOF) high-fidelity dynamic model of the system. A series of underwater experiments were carried out in a controlled environment to test the standard motion patterns of the AUV with a Proportional-Integral-Derivative (PID) controller. The performance of the PID controller will be used as the baseline for comparison of more advanced control schemes. The experimental results demonstrated that the spherical AUV was able to realize the tested underwater motions with notable performance.**

I. INTRODUCTION

A. Motivation

In Europe, there are an estimated 30,000 inactive mining stations from which a considerable number of them still contain raw materials, currently in critical demand [1]. Among these sought after raw materials there are metallic and industrial minerals, construction materials, and base metals, such as cobalt, gallium, indium and a range of rare earths necessary for IT appliances [7]. Mining operations for such materials are typically performed in underground tunnels and prolonged over long periods of time. In normal operation conditions, surface and groundwaters filter into the mined tunnels and must be constantly removed to maintain a safe working environment. Once a mine is permanently closed, the dewatering systems cease to operate and without the existence of any drainage, the tunnels become permanently submerged.

Most of these mine sites, nowadays submerged, are more than a century old which limits the information available regarding the structural layout of the tunnels. Due to the intricate network of tunnels inside a mine site and mostly unknown topology, surveying and prospecting by conventional methods such as human divers, can result dangerous or even lethal in unknown deep mine conditions [1]. Therefore, non-invasive underwater robotic platforms, in particular Autonomous Underwater Vehicles (AUVs) for geological and mineralogical studies and exploration tasks in abandoned mines, can provide important information and new data to determine whether a mine is suitable to be drained and re-opened without any major costs.

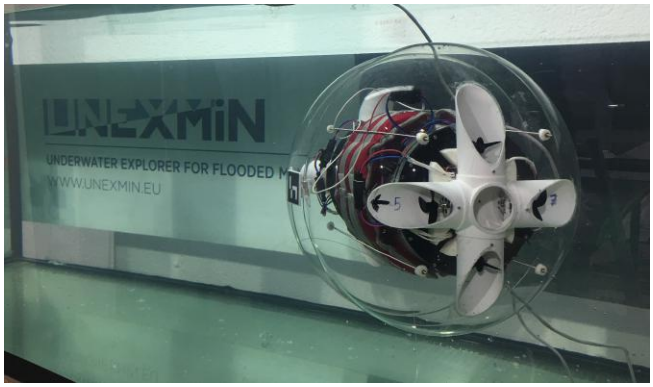

Fig. 1: Proposed spherical underwater vehicle prototype during pool tests.

Navigating with underwater vehicles inside mine environments, mostly made up of enclosed spaces (barely wide enough to fit a human), is a challenging task. Mine tunnels may contain objects or debris left after closure, which could obstruct paths or become entangled in the AUVs propellers and permanently disable the robot. Therefore, operating in these demanding environments implies certain design requirements that must be met to safely accomplish any tasks, e.g. it must be capable of moving in cluttered spaces with high maneuverability and no protruding elements to avoid becoming snared. Among several design ideas, a spherical profile for the hull was chosen.

B. Related Works

AUVs have become an active area of research in recent years due to its impact in marine economy and science in addition to maritime security and military usage [23]. The most common applications of underwater robotics include ocean mining exploration [9], autonomous sea floor mapping [10][15], and data gathering [12][13][14]. Most of these applications take place in open water environments where restrictions on shapes and sizes of the AUVs are not necessarily enforced.

Nevertheless, by adopting a streamlined spherical design, high stability and flexibility can be obtained along with a zero degree turn radius for high maneuverability and lower drag forces [8]. Several works on AUVs are found in the literature that have opted for a spherical hull design for the underwater

*This work was supported by the UNEXMIN project with funding from the European Union's Horizon 2020 research and innovation programme under Grant Agreement No. 690008, and has been co-funded by the RoboCity2030-III-CM project (Robotica aplicada a la mejora de la calidad de vida de los ciudadanos. fase III; S2013/MIT-2748), funded by Programas de Actividades I+D en la Comunidad de Madrid and co-funded by Structural Funds of the EU.

[1]Centre for Automation and Robotics (CAR), Universidad Politecnica de Madrid, Madrid, Spain. fernandez.suarez.ramon@gmail.com

robot. The University of Hawaii developed ODIN-III [20], a prototype robot with a hollow metal sphere housing of 0.315m in radius and a propulsion system that consisted of 8 screw propellers fixed outside the hull. In [16] and [19] the authors develop spherical underwater robots SUR-II and SUR-III which use water-jet thrusters as propulsion and accomplish 3 DOF motions. A micro AUV of 0.075m in radius and 6 propellers around the hull was developed by the authors of [21] and [22] for monitoring sub-surface cluttered environments as in nuclear storage ponds.

One key disadvantage of these AUV designs is the presence of external propulsion systems which could become entangled with objects such as ropes or cables encountered during operation. Taking into account the benefits and drawbacks of these systems, the design proposed in this work shown in Fig. 1, integrates the propulsion elements into the spherical hull to avoid foreign objects from damaging the propellers and effectively eliminating the possibility of ensnarement.

C. Contributions and Outline

This paper focuses on three aspects, the mechanical and electrical design of a spherical AUV prototype, the derivation of the equations of motion that describe the dynamics of the system and the implementation of a baseline controller for performance analysis in real underwater experiments. Section II will explain the mechanical design of the AUV while in Section III the equations of motion are derived. Section IV will introduce the control scheme utilized for the underwater experimental tests shown in Section V. Finally, the discussions will be explained in Section VI with conclusions and future works presented in Section VII.

II. MECHANICAL AND ELECTRONIC DESIGN

The AUV was designed to be mainly used in flooded tunnels, with dangerous areas and difficult access, therefore the design was focused on obtaining high maneuverability and an optimal shape; thus allowing the AUV to avoid stagnation in narrow or salient areas, proper to the conditions in which it will be used. Considering this was a prototype version of the real AUV, only used for control algorithm design and testing, off-the-shelf mechanical and electronic components were used which allow adding or replacing any component depending on specific needs during development.

The design of the AUV, explained bellow, is divided into 5 principal components, which are: external hull, manifolds, watertight enclosure, pendulum mechanism (used for pitch control by shifting the center of gravity (CG)) and electronic devices.

A. External Hull

One of the most widely used shapes for underwater vehicle hulls is the bullet form, like the Maya AUV [25] or ROUGHIE from Michigan Tech [28]. Although this kind of shape performs well in open water environments, it is not suitable for handling sharp turns or enclosed spaces with high maneuverability.

As mentioned before, a spherical shape for the hull offers high stability and flexibility, as well as a zero degree turn radius for maneuvering around sharp corners or avoiding obstacles in confined spaces. Furthermore, the inherent symmetry of the design provides translation in any direction without changing the heading. Fig. 1 shows the spherical hull developed for the prototype proposed in this work, it was composed of two acrylic hemispheres of 0.25m in radius fitted with the manifold system for propulsion (Section II-B) and rigidly attached to the watertight enclosure (Section II-C).

B. Manifolds

Taking into account the properties of fluid mechanics, a manifold design was chosen to enclose the propulsion system, as presented in [26]. The manifold was designed to be incorporated into the streamlined spherical shape of the hull to maximize the space available inside and avoid any protrusions from the hull or foreign objects from damaging the propellers.

As can be seen in Fig. 2, a manifold was placed on both sides of the spherical robot, each with two counter rotating vertical and horizontal motors where the use of 8 motors provides redundancy and reliability in case of any motor failure during operation. This placement allows the AUV to have 5 Degrees of Freedom (DOF), *surge* (motors {1,3,5,7}), *heave* (motors {2,4,6,8}), *yaw* (motors {1,3,5,7}), *roll* (motors {2,4,6,8}) and *sway* (motors {1,2,3,4,5,6,7,8}). Nevertheless, *roll* and *sway* motions are not considered in this work.

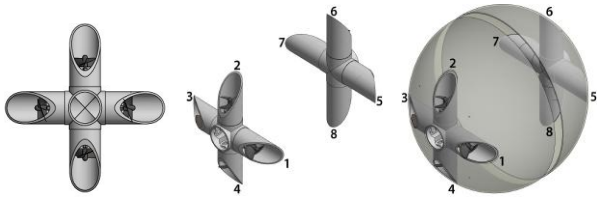

Fig. 2: (a) Front view of the manifold design. (b) Side view of the manifolds with assigned motor numbers. (c) Final placement of the manifolds in each hemisphere of the prototype AUV.

C. Watertight Enclosure

One of the most important elements when working with underwater vehicles is a watertight container in which all electronic devices susceptible to water are safe, such as: control boards, sensors, motor drivers, PC units, etc. For the spherical AUV proposed, a BlueRobotics[1] 8" Series watertight enclosure was used as shown in Fig. 3. It is made up of an acrylic tube of 6.35mm in thickness and 304.8mm in length, two aluminum O-ring flanges and two 6mm thick aluminum end caps with watertight cable penetrators, which support up to 40m depth and 392.4kPa of pressure.

[1]Blue Robotics Webpage: `https://www.bluerobotics.com`

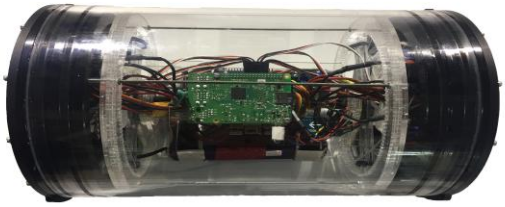

Fig. 3: Watertight Enclosure used for storing electronic devices in the proposed AUV.

D. Pendulum Mechanism

One disadvantage of using the manifold design presented in Section II-B was the loss of the *pitch* motion. Therefore, a novel pendulum mechanism was designed to change the AUVs CG by rotating a mass around the center of buoyancy (CB) of the vehicle in the forward direction, thus changing the *pitch* angle. To the authors knowledge, this is the first time this design is used for pitch control of a spherical underwater vehicle.

As seen in Fig. 4 the design consists of two fixed bases and an electronics tray rigidly mounted to the watertight enclosure's flange seal (Fig. 3); and a mobile base that is moved along the rotation axis by two DC motors and a rack-and-pinion gear design with the pinion gear attached to the DC motor and the rack gear curved along the inside of the fixed bases; thus allowing the rotation of the CG around the CB (Fig. 4 (d)) and achieving *pitch* angles from $-\pi/2$ to $\pi/2$.

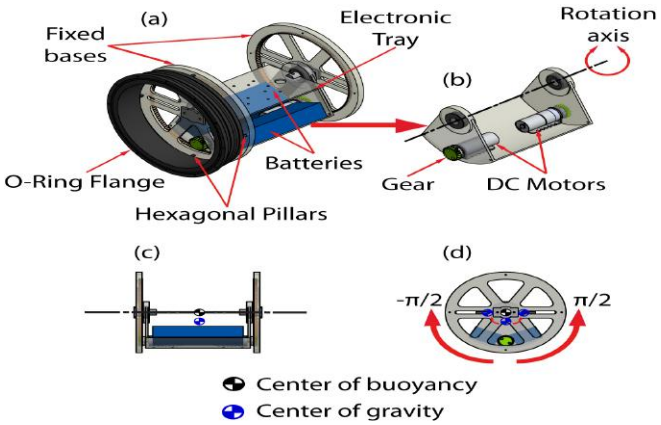

Fig. 4: (a) Complete and (b) mobile base of the pendulum mechanism, (c) front and (d) right views with the center of gravity and pitch movement.

To achieve passive stability of the vehicle without any undesired pitch or roll movements, the CG must be located lower than CB [26]. In order to move the CG below the CB, the heaviest components in the watertight enclosure, two 3S LiPo batteries (0.468kg each) used to power the vehicle were attached to the mobile base along with the DC motors (0.098kg each).

E. Electronic Devices

As explained above, the purpose of this AUV prototype is to use it as a platform in which different control architectures can be implemented for testing, prior to real scenario tests. For that reason, all the electronic equipment used are readily available products.

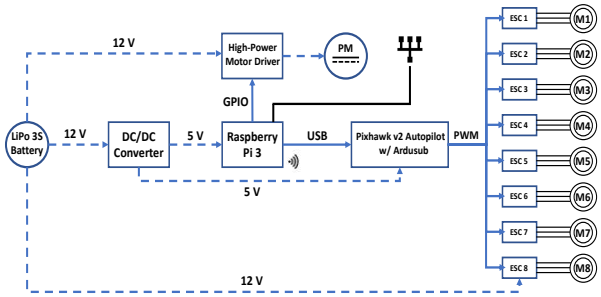

Fig. 5: Schematic of the preliminary electronic setup in the proposed AUV prototype.

The final electronic system mounted inside the watertight enclosure can be seen in Fig. 3 and the schematics in Fig. 5. The whole AUV system was powered by two 11.1V 600mAh nano-tech LiPo batteries with DC/DC converters used to power the 5V electronics. It was equipped with a Raspberry Pi 3[2] Quad Core 1.2GHz Single-board computer running Ubuntu Linux 16.04 and the Robotic-Operating-System (ROS) middleware kinetic Kame where control algorithms were implemented and executed. The on-board computer sends commands to the PixHawk v2 Autopilot [27] developed by the Computer Vision and Geometry Lab (Switzerland) with a custom firmware from the ArduSub Project[3] for low-level control and sensor measurement feedback from the 3D ACC and Gyroscope. The pendulum mechanism's DC motors were controlled by a 9 Amp Pololu high-power motor driver connected to the on-board computer through the General Purpose Input/Output (GPIO) ports available. For propulsion 8 Turnigy Aerodrive DST-700 Brushless motors were used and controlled by individual electronic speed controllers (ESC), connected to the Pixhawk's PWM output ports.

III. EQUATIONS OF MOTION

In this section the 6 DOF model for a spherical underwater vehicle is derived according to the Society of Naval Architects and Marine Engineers (SNAME) nomenclature [5]. This 6 DOF model is composed of entirely coupled equations of motion used for design and simulation tasks. Nevertheless, since the spherical AUV was not intended to have actuation in all degrees of freedom, some reduced ordered models (longitudinal model Section III-B.1 and lateral model Section III-B.2) will be presented which decouple the motions of the craft.

[2]Raspberry Pi Webpage: `https://www.raspberrypi.org`
[3]ArduSub Webpage: `https://www.ardusub.com/`

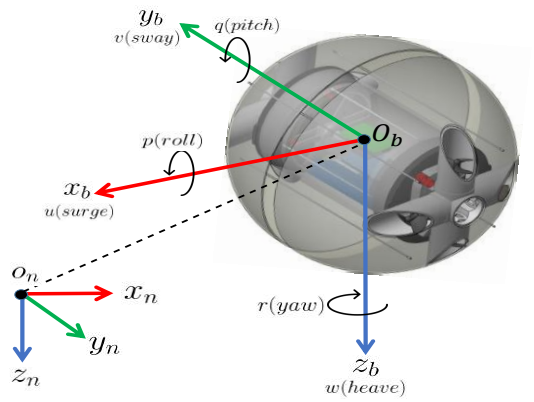

Fig. 6: AUV reference frames considered in the equations of motion. The body-fixed reference frame $\{b\}$ = $[x_b,\ y_b,\ z_b]$ with origin o_b and the North-East-Down (NED) reference frame $\{n\}$ = $[x_n,\ y_n,\ z_n]$ with origin o_n where $\{n\}$ is assumed inertial.

A. Nonlinear 6 DOF Model

The nonlinear equations of motion for a marine vehicle can be written in a vectorial setting as [3]:

$$\dot{\boldsymbol{\eta}} = \boldsymbol{J}_{\boldsymbol{\Theta}}(\boldsymbol{\eta})\boldsymbol{\nu} \tag{1}$$

$$\boldsymbol{M}\dot{\boldsymbol{\nu}} + \boldsymbol{C}(\boldsymbol{\nu})\boldsymbol{\nu} + \boldsymbol{D}(\boldsymbol{\nu})\boldsymbol{\nu} + g(\boldsymbol{\eta}) = \boldsymbol{B}\boldsymbol{\tau} \tag{2}$$

with:

$$\boldsymbol{\eta} = \begin{bmatrix} \boldsymbol{P}^n_{b/n} \\ \boldsymbol{\Theta}_{nb} \end{bmatrix} = [x, y, z, \phi, \theta, \psi]^\top \tag{3}$$

$$\boldsymbol{J}_{\boldsymbol{\Theta}}(\boldsymbol{\eta}) = \begin{bmatrix} \boldsymbol{R}^n_b(\boldsymbol{\Theta}_{nb}) & \boldsymbol{0}_{3\times3} \\ \boldsymbol{0}_{3\times3} & \boldsymbol{T}_{\Theta}(\boldsymbol{\Theta}_{nb}) \end{bmatrix} \tag{4}$$

$$\boldsymbol{\nu} = \begin{bmatrix} \boldsymbol{v}^b_{b/n} \\ \boldsymbol{\omega}^b_{b/n} \end{bmatrix} = [u, v, w, p, q, r]^\top \tag{5}$$

$$\boldsymbol{\tau} = \begin{bmatrix} \boldsymbol{f}^b_b \\ \boldsymbol{m}^b_b \end{bmatrix} = [X, Y, Z, K, M, N]^\top \tag{6}$$

where $\boldsymbol{\eta} \in \mathbb{R}^3 \times \mathcal{S}^3$ denotes the position and orientation vector in the NED coordinate system (Fig. 6). In (3) the position vector $\boldsymbol{P}^n_{b/n} \in \mathbb{R}^3$ is defined as the distance of the point o_b with respect to $\{n\}$ expressed in $\{n\}$ and $\boldsymbol{\Theta}_{nb} \in \mathcal{S}^3$ is a vector of Euler angles between $\{n\}$ and $\{b\}$. $\boldsymbol{J}_{\boldsymbol{\Theta}}(\boldsymbol{\eta})$ is a 6×6 transformation matrix consisting of a rotation matrix $\boldsymbol{R}^n_b(\boldsymbol{\Theta}_{nb})$, for transforming linear velocities in $\{b\}$ to $\{n\}$, and a transformation matrix $\boldsymbol{T}_{\Theta}(\boldsymbol{\Theta}_{nb})$ to relate the angular velocities $\boldsymbol{\omega}^b_{b/n}$ in $\{b\}$ to the Euler rate vector $\dot{\boldsymbol{\Theta}}_{nb}$. In (5), $\boldsymbol{\nu} \in \mathbb{R}^6$ denotes the linear and angular velocity vectors in the body-fixed reference frame and $\boldsymbol{\tau} \in \mathbb{R}^6$ is used to describe the forces and moments acting on the vehicle in the body-fixed reference frame with $\boldsymbol{B}$ used as a mapping matrix for thruster configuration.

1) System Inertia Matrix: The system inertia matrix (7) is a positive semi-definite matrix composed of the rigid-body inertia matrix $\boldsymbol{M}_{RB}$ and the added mass inertia matrix $\boldsymbol{M}_A$.

$$\boldsymbol{M} = \boldsymbol{M}_{RB} + \boldsymbol{M}_A, \quad \boldsymbol{M} = \boldsymbol{M}^\top > 0 \tag{7}$$

In the case of a spherical vehicle with symmetry in the xz, yz and xy planes, the rigid-body matrix takes the form:

$$\boldsymbol{M}_{RB} = \boldsymbol{M}^\top_{RB} \approx diag\{m, m, m, I_{xx}, I_{yy}, I_{zz}\} \tag{8}$$

where m is the mass of the vehicle and $\{I_{xx}, I_{yy}, I_{zz}\}$ are the moments of inertia about the $\{b\}$ axes. The 6×6 inertia matrix of added mass terms is explained in detail in [2]. Given that most AUV applications restrict the vehicle to slow speeds maneuvers and the fact that the vehicle has three planes of symmetry, the contribution of the off-diagonal elements in the added mass inertia matrix $\boldsymbol{M}_A$ can be neglected. Hence,

$$\boldsymbol{M}_A = \boldsymbol{M}^\top_A \approx -diag\{X_{\dot{u}}, Y_{\dot{v}}, Z_{\dot{w}}, K_{\dot{p}}, M_{\dot{q}}, N_{\dot{r}}\} \tag{9}$$

The added mass matrix elements $X_{\dot{u}}$, $Y_{\dot{v}}$, $Z_{\dot{w}}$, $K_{\dot{p}}$, $M_{\dot{q}}$ and $N_{\dot{r}}$ are the hydrodynamic added mass forces as explained in [2]. Furthermore, (9) describes the mass that the AUV has to displace while moving and the added inertia due to the displaced mass while rotating. The spherical AUV does not create any mass displacement while rotating and consequently the last three elements of (9) can be approximated to zero.

2) Coriolis-Centripetal Matrix: The Coriolis and Centripetal term matrix (10) is caused by the rotation of the body with respect to the inertial reference frame.

$$\boldsymbol{C}(\boldsymbol{\nu}) = \boldsymbol{C}_{RB}(\nu) + \boldsymbol{C}_A(\nu) \tag{10}$$

$\boldsymbol{C}_{RB}(\nu)$ and $\boldsymbol{C}_A(\nu)$ are the rigid-body and hydrodynamic Coriolis and Centripetal matrices respectively. The theory and proofs of these matrices is beyond the scope of this paper but can be found thoroughly explained in literature [3]. It is generally good practice to design the system with the center of gravity (CG) located lower than the center of buoyancy (CB) in order to stabilize the system. For the spherical AUV if the CG and the CB are located vertically on the z axis, that is, $x_b = x_g \approx 0$ and $y_b = y_g \approx 0$ and I_{xy}, I_{xz}, $I_{yz} \approx 0$, the rigid-body Coriolis and Centripetal matrix is defined as:

$$\boldsymbol{C}_{RB}(\boldsymbol{\nu}) = \begin{bmatrix} 0 & 0 & 0 & mz_g r & mw & -mv \\ 0 & 0 & 0 & -mw & mz_g r & mu \\ 0 & 0 & 0 & -m\alpha_1 & -m\alpha_2 & 0 \\ -mz_g r & mw & m\alpha_1 & 0 & I_z r & -I_y q \\ -mw & -mz_g r & m\alpha_2 & -I_z r & 0 & I_x p \\ mv & -mu & 0 & I_y q & -I_x p & 0 \end{bmatrix} \tag{11}$$

with

$$\alpha_1 = (z_g p - v), \quad \alpha_2 = (z_g q + u). \tag{12}$$

The nonlinear hydrodynamic Coriolis and Centripetal matrix $\boldsymbol{C}_A(\boldsymbol{\nu})$ due to a rotation of the body reference

frame about the inertial frame can be derived using an energy formulation based on the added mass matrix $\boldsymbol{M}_A$ [2].

$$\boldsymbol{C}_A(\boldsymbol{\nu}) \begin{bmatrix} 0 & 0 & 0 & 0 & -Z_{\dot{w}}w & Y_{\dot{v}}v \\ 0 & 0 & 0 & Z_{\dot{w}}w & 0 & -X_{\dot{u}}u \\ 0 & 0 & 0 & -Y_{\dot{v}}v & X_{\dot{u}}u & 0 \\ 0 & -Z_{\dot{w}}w & Y_{\dot{v}}v & 0 & -N_{\dot{r}}r & M_{\dot{q}}q \\ Z_{\dot{w}}w & 0 & -X_{\dot{u}}u & N_{\dot{r}}r & 0 & -K_{\dot{p}}p \\ -Y_{\dot{v}}v & X_{\dot{u}}u & 0 & -M_{\dot{q}}q & K_{\dot{p}}p & 0 \end{bmatrix} \tag{13}$$

3) Damping Matrix: The total hydrodynamic damping matrix $\boldsymbol{D}(\boldsymbol{\nu})$ is the sum of the linear term $\boldsymbol{D}$ and the nonlinear term $\boldsymbol{D}_n(\boldsymbol{\nu})$ such that,

$$\boldsymbol{D}(\boldsymbol{\nu}) = \boldsymbol{D} + \boldsymbol{D}_n(\boldsymbol{\nu}). \tag{14}$$

If the underwater vehicle is maneuvering at low speeds and the motions are considered uncoupled, $\boldsymbol{D}(\boldsymbol{\nu})$ could be assumed mathematically as [3]:

$$\begin{aligned} \boldsymbol{D}(\boldsymbol{\nu}) = &-diag\{X_u, Y_v, Z_w, K_p, M_q, N_r\} \\ &- diag\{X_{|u|u}|u|, Y_{|v|v}|v|, Z_{|w|w}|w|, \\ &K_{|p|p}|p|, M_{|q|q}|q|, N_{|r|r}|r|\} \end{aligned} \tag{15}$$

where the damping coefficients in (15) as well as (13) are using the SNAME notation and are called hydrodynamic derivatives. Definitions and theory can be found in [4].

4) Vector of Gravitational Forces and Moments: Conforming to the SNAME nomenclature, the weight and buoyancy of a submerged vehicle is given by

$$W = mg, \quad B = \rho g \nabla \tag{16}$$

where g is the acceleration of gravity in NED, ∇ is the volume of fluid displaced by the vehicle and ρ is the density of water. As in Section III-A.2, if $x_b = x_g \approx 0$ and $y_b = y_g \approx 0$, the Euler angle representation of hydrostatic forces and moments for the gravitational and buoyant forces acting on the vehicle is given by [2]:

$$\boldsymbol{g}(\boldsymbol{\nu}) = \begin{bmatrix} (W-B)\sin\theta \\ -(W-B)\cos\theta\sin\phi \\ -(W-B)\cos\theta\cos\phi \\ (z_gW - z_bB)\cos\theta\sin\phi \\ (z_gW - z_bB)\sin\theta \\ 0 \end{bmatrix} \tag{17}$$

As can be seen in (17) if the underwater vehicle is close to neutrally buoyant ($W = B$), the gravitational forces only affect the rotations in the x and y axes.

B. Reduced Order Models

In certain cases the nonlinear equations of motion presented in Section III-A can be divided into two slightly interacting subsystems. In the longitudinal subsystem the states are chosen to be $\{u, w, q, \theta\}$ while the remaining states (e.g. $\{v, p, r, \phi, \psi\}$) are those of the lateral subsystem. From the diagonal structure of (7)-(9), it can be observed in (18) that the two subsystems are clearly decoupled.

$$\boldsymbol{M}_{long} = \begin{bmatrix} M_{11} & 0 & 0 \\ 0 & M_{33} & 0 \\ 0 & 0 & M_{55} \end{bmatrix} \boldsymbol{M}_{lat} = \begin{bmatrix} M_{22} & 0 & 0 \\ 0 & M_{44} & 0 \\ 0 & 0 & M_{66} \end{bmatrix} \tag{18}$$

1) Longitudinal Model: In the longitudinal model, the states of the lateral subsystem are assumed to be small ($v = p = r = \phi = \psi \approx 0$). Therefore, the longitudinal kinematics for u, w and θ are [2],

$$\begin{bmatrix} \dot{x} \\ \dot{z} \\ \dot{\theta} \end{bmatrix} = \begin{bmatrix} \sin\theta & 0 \\ \cos\theta & 0 \\ 0 & 1 \end{bmatrix} \begin{bmatrix} w \\ q \end{bmatrix} + \begin{bmatrix} \cos\theta \\ -\sin\theta \\ 0 \end{bmatrix} u \tag{19}$$

To reduce the complexity of the system, the higher order damping terms $\boldsymbol{D}_n(\boldsymbol{\nu})$ in (14) are neglected. Nevertheless, the Coriolis-Centripetal matrix (10) is modeled assuming that v, w, p, q and r are small and $u >> 0$. Thus, using (11) - (13).

$$\boldsymbol{C}_{RB}(\boldsymbol{\nu})\boldsymbol{\nu} \approx \begin{bmatrix} 0 & 0 & 0 \\ 0 & 0 & -mu \\ 0 & 0 & 0 \end{bmatrix} \begin{bmatrix} u \\ w \\ q \end{bmatrix} \tag{20}$$

$$\boldsymbol{C}_A(\boldsymbol{\nu})\boldsymbol{\nu} \approx \begin{bmatrix} 0 & 0 & 0 \\ 0 & 0 & X_{\dot{u}}u \\ 0 & (Z_{\dot{w}} - X_{\dot{u}})u & 0 \end{bmatrix} \begin{bmatrix} u \\ w \\ q \end{bmatrix} \tag{21}$$

Therefore, according to (2), (7), (15), (17), the dynamics become

$$\begin{aligned} &\begin{bmatrix} m - X_{\dot{u}} & 0 & 0 \\ 0 & m - Z_{\dot{w}} & 0 \\ 0 & 0 & I_y - M_{\dot{q}} \end{bmatrix} \begin{bmatrix} \dot{u} \\ \dot{w} \\ \dot{q} \end{bmatrix} + \begin{bmatrix} -X_u & 0 & 0 \\ 0 & -Z_w & 0 \\ 0 & 0 & -M_q \end{bmatrix} \begin{bmatrix} u \\ w \\ q \end{bmatrix} \\ &+ \begin{bmatrix} 0 & 0 & 0 \\ 0 & 0 & \gamma_1 u \\ 0 & (Z_{\dot{w}} - X_{\dot{u}})u & 0 \end{bmatrix} \begin{bmatrix} u \\ w \\ q \end{bmatrix} + \begin{bmatrix} (W-B)s\theta \\ -(W-B)c\theta c\phi \\ (z_gW - z_bB)s\theta \end{bmatrix} = \boldsymbol{B} \begin{bmatrix} \tau_1 \\ \tau_3 \\ \tau_5 \end{bmatrix} \end{aligned} \tag{22}$$

for $\gamma_1 = (X_{\dot{u}} - m)$.

2) Lateral model: For the lateral model, the longitudinal subsystem states $\{u, w, q$ and $\theta\}$ and the roll angle (ϕ) are assumed to be small. The lateral kinematis result in

$$\begin{bmatrix} \dot{y} \\ \dot{\phi} \\ \dot{\psi} \end{bmatrix} = \begin{bmatrix} \cos\psi & 0 & 0 \\ 0 & 1 & 0 \\ 0 & 0 & 1 \end{bmatrix} \begin{bmatrix} v \\ p \\ r \end{bmatrix} \tag{23}$$

As in the previous section (III-B.1), the higher order terms in (14) are neglected and the Coriolis terms in (10) are modeled assuming that v, w, p, q and r are negligible. Hence from (11) - (13).

$$\boldsymbol{C}_{RB}(\boldsymbol{\nu})\boldsymbol{\nu} \approx \begin{bmatrix} 0 & 0 & mu \\ 0 & 0 & -mz_gu \\ 0 & 0 & 0 \end{bmatrix} \begin{bmatrix} v \\ p \\ r \end{bmatrix} \tag{24}$$

$$\boldsymbol{C}_A(\boldsymbol{\nu})\boldsymbol{\nu} \approx \begin{bmatrix} 0 & 0 & -X_{\dot{u}}u \\ 0 & 0 & 0 \\ (X_{\dot{u}} - Y_{\dot{v}})u & 0 & 0 \end{bmatrix} \begin{bmatrix} v \\ p \\ r \end{bmatrix} \tag{25}$$

Therefore, the dynamics of the lateral subsystem become

$$\begin{aligned} &\begin{bmatrix} m - Y_{\dot{v}} & 0 & 0 \\ 0 & I_x - K_{\dot{p}} & 0 \\ 0 & 0 & I_z - N_{\dot{r}} \end{bmatrix} \begin{bmatrix} \dot{v} \\ \dot{p} \\ \dot{r} \end{bmatrix} + \begin{bmatrix} -Y_v & 0 & 0 \\ 0 & -K_p & 0 \\ 0 & 0 & -N_r \end{bmatrix} \begin{bmatrix} v \\ p \\ r \end{bmatrix} \\ &+ \begin{bmatrix} 0 & 0 & \gamma_2 u \\ 0 & 0 & -mz_gu \\ \gamma_4 u & 0 & 0 \end{bmatrix} \begin{bmatrix} v \\ p \\ r \end{bmatrix} + \begin{bmatrix} -(W-B)c\theta s\phi \\ \gamma_3 c\theta s\phi \\ 0 \end{bmatrix} = \boldsymbol{B} \begin{bmatrix} \tau_2 \\ \tau_4 \\ \tau_6 \end{bmatrix} \end{aligned} \tag{26}$$

where, $\gamma_2 = (m - X_{\dot{u}}); \gamma_3 = (z_gW - z_gB); \gamma_4 = (X_{\dot{u}} - Y_{\dot{v}})$.

IV. CONTROL SYSTEM DESIGN

This spherical AUV prototype will be used to test advanced control algorithms before implementing them in the real robotic system deployed in the mine sites. Therefore, a benchmark performance evaluation of the AUV was needed for the purpose of comparison with other control methods implemented in future experimental tests. Due to the success achieved by Proportional-Integral-Derivative (PID) controller implementations in the literature [17] [18], it was only logical that the controller chosen as the baseline for comparison was the PID controller. The control loop was implemented using position as feedback inputs and an ideal form PID controller (greater tuning methods flexibility) [24], which is shown in (27).

$$u(t) = k_p\left(e(t) + \frac{1}{T_i}\int_0^t e(\tau)d\tau + T_d\frac{de}{dt}\right) \tag{27}$$

where u is the control signal composed of, T_i and T_d, the integral and derivative time constants and k_p is the proportional gain. For the experiments shown in Section V, the Ziegler-Nichols tunning technique was applied initially to obtain baseline values of PID controller gains and afterwards finely tuned during underwater tests. The innovation presented in this work is not from the type of control method being implemented, but the effects and validation of the AUV prototype it is implemented on.

V. EXPERIMENTS

A. Experimental Setup

The overall goal of the inspection tasks inside the mines is to gather measurements from scientific instruments for analysis, hence, in most occasions the AUV must maintain a desired position for the data not to be corrupted, e.g. photos from multi-spectral cameras not to be blurred. Thus, to simulate future measurement acquisition tasks, the tests performed were specifically testing the ability of the AUV to move to a precise position and maintain this location, also known as a regulation problem [24].

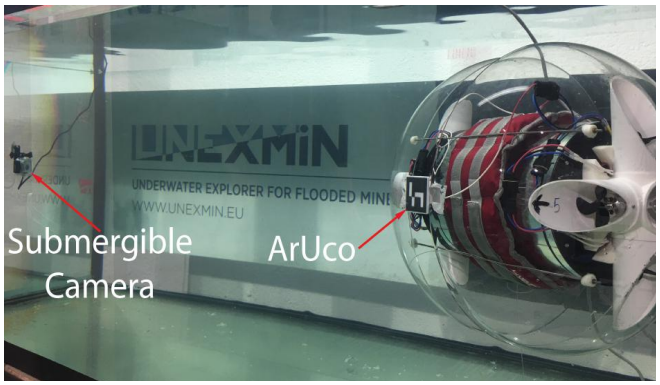

Fig. 7: Experimental setup used during test. A 2m×1m×1m glass tank was used to test the basic motions of the AUV in controlled underwater scenario.

Experiments were carried out in a 2m×1m×1m glass tank and the position hold performance of the proposed AUV was evaluated in several underwater tests. Based on the experimental results presented in [6] and [11], an artificial fiducial marker (ArUco [29]) was placed on the AUV to determine the pose of the vehicle w.r.t the submersible's camera reference frame which was installed inside the tank, as shown in Fig. 7. The pose obtained from the visual marker was found to have sufficient precision to be used as position and orientation feedback for the PID controllers in surge, heave and yaw motions. All hardware interfaces have been implemented in Python or c++ under the standard c++11 in Ubuntu 16.04 and data communications are handled using the ROS[4] middleware standard messages.

As can be seen in (16) the buoyancy of the vehicle depends on the volume of fluid displaced by the body. In the case of the AUV proposed, the buoyancy is much larger than the weight of the vehicle and thus dead weights must be added in order to obtain approximate neutral buoyancy. Lead weights were added in the flanges, inside the watertight enclosure in addition to a sand bag weight around the watertight container for a total of 6kg in dead weight. For real time data visualization, acquisition and tuning, a tether cable was used in the initial tests since low frequency wireless communication modules were not available.

B. Underwater Decoupled Experiments

The longitudinal model states of the AUV dynamic model, shown in Section III-B.1, as well as the yaw angle, were individually tested to measure the performance of each DOF without unwanted disturbances caused by coupled motions.

1) Surge: The surge (u) motion test was performed to verify and validate the vehicle movement in the North direction (x axis) of the AUV. During the test, the yaw angle was manually adjusted if any deviation from the heading was observed due to motor manufacturing differences. Multiple position reference commands were sent to analyze the forward and backward movement of the AUV. Fig. 8(a) shows the position displacement in the North direction for the AUV surge motion test. First, the AUV was given a reference of 0.5m which is movement in the forward direction towards the frame of the camera and after several position references in each direction, the AUV is sent back to the initial position.

2) Pitch: The duration of the pitch (θ) motion experiments was approximately 188s. During this time the AUV was given steps in forward angle references of -30 degrees (nose down) and backward references of +45 degrees (nose up). In view of the good quality of the pitch angle measurements provided by the Pixhawk autopilot, these values were used as feedback measurements for the controller. The angle output of the AUV to the reference step commands is shown in Fig. 8(b).

3) Yaw: In Fig. 8(c) the results for the yaw (ψ) experimental test are presented. Unlike the pitch angles, the yaw angle provided by the Pixhawk autopilot presented considerable drift despite having an Extended Kalman Filter (EKF) for yaw estimation. Thus, for this motion test, angle reference commands were sent and the feedback taken from the fiducial marker localization system.

4) Heave: In the heave (w) motion test, multi-depth references were applied to the AUV to analyze the performance of the vehicle in maintaining depth positions. The results obtained and the depth references setpoints are shown in Fig. 8(d). The depth commands in the heave experimental test were limited to small displacements, this was due to the field of view of the camera, as well as the size of the test tank in relation to the size of the robot, similar to the surge tests performed in Section V-B.1.

C. Underwater Coupled Experiments

To test the effects of coupled motion dynamics in the performance of the AUV, the yaw and the heave movements were tested simultaneously. The test was performed for a duration of 80s and a disturbance was added at 14.5s and terminated at 24.5s to evaluate the response. The yaw was given a fixed reference of 120 degrees for the entire duration of the test. The initial depth reference was to maintain the AUV at 0m (the center of the image in the submersible camera) and afterwards a step reference was commanded. The results for this test can be seen in Fig. 8(e) for yaw and Fig. 8(f) for depth.

[4]ROS Webpage: `https://www.ros.org/`

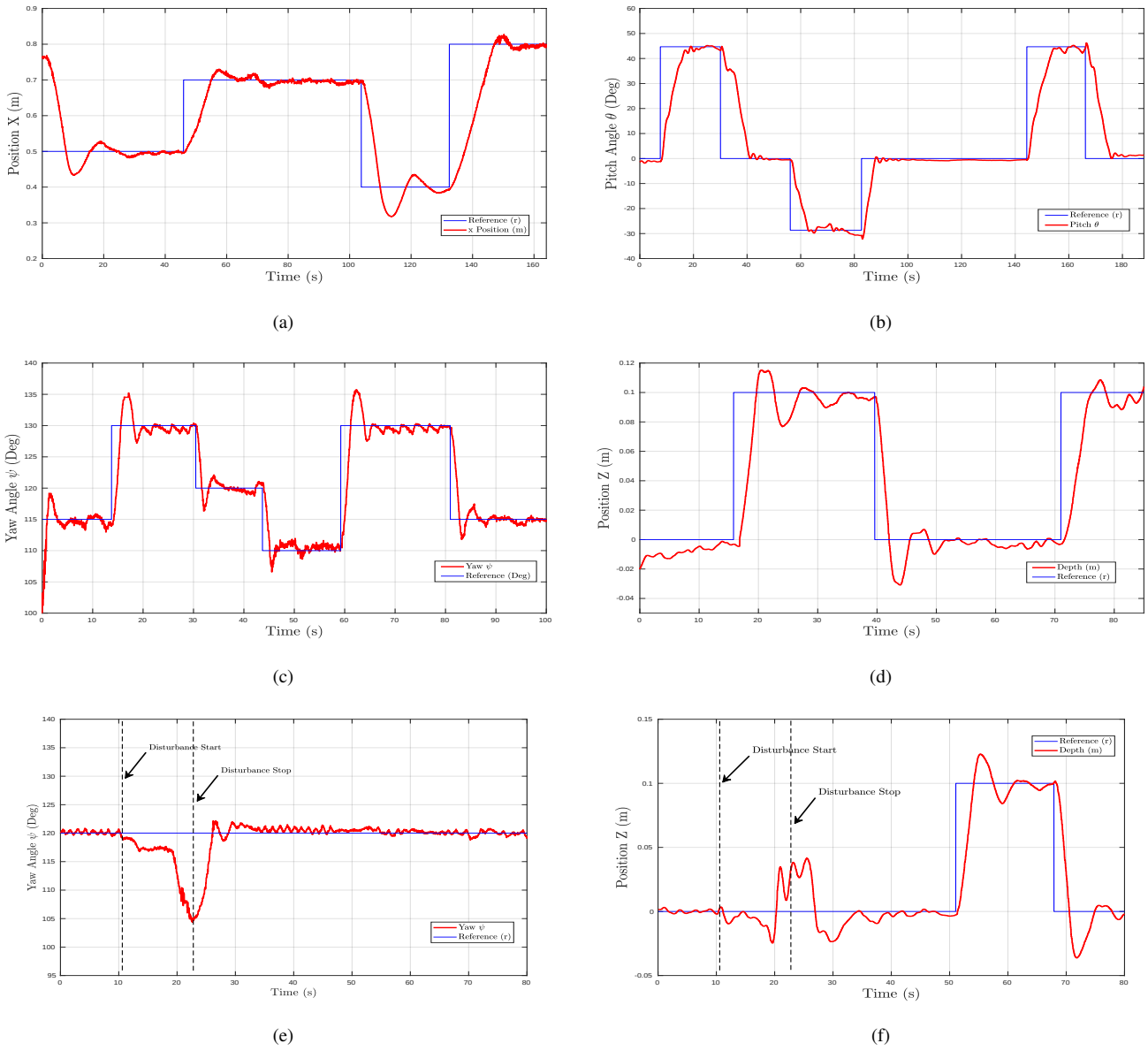

Fig. 8: Experimental results obtained in underwater decoupled tests: (a) Surge (u), (b) Pitch (θ), (c) Yaw (ψ) and (d) Depth (w). (e) Yaw and (f) Depth decoupled experiment results with added disturbance at t = 14.5s and terminated at t = 24.5s.

VI. DISCUSSION

In the previous section, the underwater experiments performed were summarized and the basic methodology used in the tests was explained. The experiments were divided into coupled and decoupled underwater tests of the longitudinal and yaw motions of the AUV. The average time response analysis results for the decoupled experimental tests are shown in Table I, where $OS\%$ is the Overshoot percentage, T_r is the Rise time, T_f is the Fall time, T_s is the Settling time and eSS is the Steady-State error.

As can be observed, the linear movements of the AUV (x and z directions) showed very similar results for the metrics evaluated. This behavior was to be expected since the AUV is symmetric in all three planes and thus must have similar dynamics in the linear motions. One key difference in the results of the linear motions was the T_f, where the value for the z direction was significantly larger. This was due to the negative buoyancy of the AUV with the added ballasts. Since the vehicle was not neutrally buoyant, the force of the weight on the vehicle made it dive fast, averaging a lower T_f.

TABLE I: Time Response Results in Decoupled Experiments

Metrics	North (x)	Pitch (θ)	Yaw (ψ)	Down (z)	Units
$OS\%$	13.16	1.28	4.24	15.10	[%]
T_r	3.04	7.05	1.11	2.74	[s]
T_f	6.83	8.59	1.34	1.70	[s]
T_s	24.94	16.34	7.83	17.80	[s]
eSS	0.0083 (m)	1.53 (deg)	0.6522 (deg)	0.0063 (m)	[-]

However, the results in the North direction shown in Fig. 8(a) presented much less oscillatory behavior in Steady-State (SS) and a faster T_r than the Down motion (as mentioned before due to the buoyancy of the vehicle). Nonetheless, both linear motions obtained significantly low errors in SS even with the uncertainty introduced by the visual marker based pose estimation.

The experimental results on the rotational motions of the AUV can be seen in Fig. 8(b) and Fig. 8(c). The yaw controller provided an eSS of 0.6522 deg, a T_r of 1.11s and an $OS\%$ of 4.24% all very desirable values. Nevertheless, the response showed oscillatory behavior in SS with a constant frequency and amplitude around the reference angle set at 130 degrees. Since this behavior has been previously seen in underwater systems controlled with PID controllers [24], these oscillations could either be caused by the controller or by a faulty detection of the visual marker which introduces errors in the measurements. The pitch outputs validate the pendulum mechanism design proposed in this work. Results demonstrate excellent transient and stationary behavior with the lowest $OS\%$ 1.28% and overall less oscillatory behavior in SS as can be seen in Fig. 8(c). Therefore, the design implemented in this vehicle can be validated and accepted as a valid solution for pitch control of a spherical underwater vehicle.

The performance of the coupled motion experiments can be seen in Fig. 8(e) and Fig. 8(f) for yaw and z respectively. Similar to the results obtained in the decoupled test for yaw, the output signal presented oscillations in SS but low errors in SS and good rejection to the disturbances added. The z response was also satisfactory and similar to the coupled test results with acceptable rejection to unknown disturbances and very low eSS values.

VII. CONCLUSIONS AND FUTURE WORK

In this paper, a design of a spherical autonomous underwater robot prototype for mine tunnel exploration was presented. The mechanical and electrical designs have been custom made including the development of a novel pendulum mechanism for pitch control and a manifold system for propulsion. The 6 DOF equations of motion for the AUV have been derived and simplified to reduced ordered models of longitudinal and lateral states. Surge, heave, pitch and yaw motions were tested in real underwater experiments with a baseline PID controller and visual marker pose feedback. The AUVs performance was evaluated for both coupled and decoupled motions in position hold tests. Results demonstrate that the proposed design of the AUV has notable performance with very acceptable steady-state errors.

Future work on the development of this prototype includes testing low frequency communication modules for wireless operation, implementation and validation of advanced control techniques such as sliding mode control and $\mathcal{L}_1$ Adaptive Control and sensor fusion algorithms to enhance the localization of the AUV in underwater tests.

SUPPLEMENTARY MATERIAL

Video of the experiments: `https://vimeo.com/259423959`

REFERENCES

[1] UNEXMIN.eu, 'Project Overview: Developing science and technology', 2016. [Online]. Available: http://www.unexmin.eu/the-project/project-overview/. [Accessed: 01- Mar- 2018].

[2] Fossen, T. I, Handbook of marine craft hydrodynamics and motion control, New York: John Wiley and Sons. (2011).

[3] Fossen, T. I, Nonlinear Modeling and Control of Underwater Vehicles. PhD thesis. Department of Engineering Cybernetics, Norwegian University of Science and Technology. Trondheim, Norway. (1991).

[4] Michio Ueno, Hydrodynamic derivatives and motion response of a submersible surface ship in unbounded water, Ocean Engineering, Volume 37, Issue 10, 2010, Pages 879-890.

[5] SNAME (1950). The Society of Naval Architects and Marine Engineers. Nomenclature for Treating the Motion of a Submerged Body Through a Fluid. In: Technical and Research Bulletin No. 125.

[6] D. B. dos Santos Cesar, C. Gaudig, M. Fritsche, M. A. dos Reis and F. Kirchner, "An evaluation of artificial fiducial markers in underwater environments," OCEANS 2015 - Genova, Genoa, 2015.

[7] Opinion of the European Economic and Social Committee on 'Securing essential imports for the EU - through current EU trade and related policies'. (2014). Official Journal of the European Union. C67, 47-53.

[8] Y. Li, S. Guo and C. Yue, "Study on the control system of a novel spherical underwater robot", 2015 IEEE International Conference on Mechatronics and Automation (ICMA), Beijing, 2015, pp. 2100-2105.

[9] W. Senke, "Applications of autonomous underwater vehicles (AUVs) in ocean mining exploration," 2013 OCEANS - San Diego, San Diego, CA, 2013, pp. 1-3.

[10] K. Bergh nonsen, O. K. Hagen and E. Berglund, "Autonomous mapping with AUVs using relative terrain navigation," OCEANS 2017 ? Anchorage, Anchorage, AK, 2017, pp. 1-7.

[11] M. Caccia, Vision-based ROV horizontal motion control: Near-seafloor experimental results, Control Engineering Practice, Volume 15,Issue 6,2007,Pages 703-714.

[12] Xuri Yu, Tommy Dickey, James Bellingham, Derek Manov, Knut Streitlien, The application of autonomous underwater vehicles for interdisciplinary measurements in Massachusetts and Cape Cod Bays, Continental Shelf Research,Volume 22,Issue 15,2002.

[13] Fernandes, P.G., Brierley, A.S., Simmonds, E.J., Millard, N.W., McPhail, S.D., Armstrong, F., Stevenson, P., Squires, M., 2000. Fish do not avoid survey vessels. Nature 404, 35?36.

[14] Nadis, S., 1997. Real time oceanography adapts to sea changes. Science 275, 1881?1882.

[15] Roman, Chris, Singh, Hanumant, A Self-Consistent Bathymetric Mapping Algorithm, Journal of Field Robotics, 2007

[16] Yaxin Li, Shuxiang Guo, Yu Wang, Design and characteristics evaluation of a novel spherical underwater robot, Robotics and Autonomous Systems, Volume 94, 2017.

[17] HOLTZHAUSEN, S. D. Design of an autonomous underwater vehicle: vehicle tracking and position control. University of KwaZulu-Natal, Master?s Thesis. 2010.

[18] S.B. Williams,P. Newman,G. Dissanayake, J. Rosenblatt and H. Durrant-Whyte, A Decoupled, Distributed AUV Control Architecture, International Symposium on Robotics, 2000.

[19] C. Yue, S. Guo, M. Li and Y. Li, "Passive and active attitude stabilization method for the spherical underwater robot (SUR-II)," 2013 IEEE International Conference on Robotics and Biomimetics (ROBIO), Shenzhen, 2013, pp. 1019-1023.

[20] H. T. Choi, A. Hanai, S. K. Choi and J. Yuh, "Development of an underwater robot, ODIN-III," Proceedings 2003 IEEE/RSJ International Conference on Intelligent Robots and Systems (IROS 2003) (Cat. No.03CH37453), 2003, pp. 836-841 vol.1.

[21] S. A. Watson, D. J. P. Crutchley and P. N. Green, "The design and technical challenges of a micro-autonomous underwater vehicle (?AUV)," 2011 IEEE International Conference on Mechatronics and Automation, Beijing, 2011, pp. 567-572.

[22] Watson, Simon A. et al. ?The mechatronic design of a micro-autonomous underwater vehicle (AUV).? IJMA 2 (2012): 157-168.

[23] M. B. Loc and H. S. Choi, "Design of self-tuning gain depth controller for an autonomous underwater vehicle with mass shifter mechanism," 2012 12th International Conference on Control, Automation and Systems, JeJu Island, 2012, pp. 1742-1746.

[24] S. A. Watson and P. Green, Depth Control for Micro-Autonomous Underwater Vehicles (?AUVs): Simulation and Experimentation, International Journal of Advanced Robotic Systems,11, 2014.

[25] R. Madhan, E. S. Desa, S. Prabhudesai, L. Sebastiao, A. Pascoal, E. Desa, A. A. M. Q. Mascarenhas, P. Maurya, G. S. Navelkar,S. Afzulpurkar, and S. Khalap. Mechanical design and development aspects of a small AUV - Maya. In 7th IFAC Conference on Manoeuvring and Control of Marine Craft, MCMC, Lisbon, Portugal, 2006.

[26] S. Zavari, A. Heininen, J. Aaltonen and K. T. Koskinen, "Early stage design of a spherical underwater robotic vehicle," 2016 20th International Conference on System Theory, Control and Computing (ICSTCC), Sinaia, 2016, pp. 240-244.

[27] Lorenz Meier, Dominik Honegger and Marc Pollefeys. PX4: A Node-Based Multithreaded Open Source Robotics Framework for Deeply Embedded Platforms, ICRA (Int. Conf. on Robotics and Automation) 2015.

[28] B. R. Page, S. Ziaeefard, A. J. Pinar and N. Mahmoudian, "Highly Maneuverable Low-Cost Underwater Glider: Design and Development," in IEEE Robotics and Automation Letters, vol. 2, no. 1, pp. 344-349, Jan. 2017.

[29] S. Garrido-Jurado and R. Muñoz-Salinas and F.J. Madrid-Cuevas and M.J. Marín-Jiménez. Automatic generation and detection of highly reliable fiducial markers under occlusion, Pattern Recognition, 2014.